

# From Equilibrium to Steady-State Dynamics after Switch-On of Shear

Matthias Krüger,<sup>1</sup> Fabian Weysser,<sup>1</sup> and Thomas Voigtmann<sup>1,2,3</sup>

<sup>1</sup>*Fachbereich Physik, Universität Konstanz, 78457 Konstanz, Germany*

<sup>2</sup>*Institut für Materialphysik im Weltraum, Deutsches Zentrum für Luft- und Raumfahrt (DLR), 51170 Köln, Germany*

<sup>3</sup>*Zukunftskolleg, Universität Konstanz, 78457 Konstanz, Germany*

(Dated: February 7, 2022)

A relation between equilibrium, steady-state, and waiting-time dependent dynamical two-time correlation functions in dense glass-forming liquids subject to homogeneous steady shear flow is discussed. The systems under study show pronounced shear thinning, i.e., a significant speedup in their steady-state slow relaxation as compared to equilibrium. An approximate relation that recovers the exact limit for small waiting times is derived following the integration through transients (ITT) approach for the nonequilibrium Smoluchowski dynamics, and is exemplified within a schematic model in the framework of the mode-coupling theory of the glass transition (MCT). Computer simulation results for the tagged-particle density correlation functions corresponding to wave vectors in the shear-gradient directions from both event-driven stochastic dynamics of a two-dimensional hard-disk system and from previously published Newtonian-dynamics simulations of a three-dimensional soft-sphere mixture are analyzed and compared with the predictions of the ITT-based approximation. Good qualitative and semi-quantitative agreement is found. Furthermore, for short waiting times, the theoretical description of the waiting time dependence shows excellent quantitative agreement to the simulations. This confirms the accuracy of the central approximation used earlier to derive fluctuation dissipation ratios (Phys. Rev. Lett. **102**, 135701). For intermediate waiting times, the correlation functions decay faster at long times than the stationary ones. This behavior is predicted by our theory and observed in simulations.

PACS numbers: 82.70.Dd, 64.70.P-, 05.70.Ln, 83.60.Df

## I. INTRODUCTION

The application of shear flow to dense liquids can dramatically change their transport and relaxation processes. Even if the timescale set by the applied shear rate  $\dot{\gamma}$  is slow compared to a typical single-particle relaxation time  $\tau_0$  (i.e., the Péclet number  $Pe_0 = \dot{\gamma}\tau_0 \ll 1$ ), it can interfere with and supersede the slow relaxation times  $\tau_\alpha$  of the system (i.e., the “dressed” Péclet, or Weissenberg number  $Pe = \dot{\gamma}\tau_\alpha \gg 1$ ). In this case, the slow relaxation of the system is usually found to be accelerated by the shear flow, a phenomenon known from colloidal suspensions as shear thinning, because a pronounced decrease in the apparent viscosity results. To this decrease corresponds an increase in the single-particle diffusivities. These changes in transport processes are found even if the average static structure of the system (at least as measured through two-point correlation functions) changes only slightly.

The drastic change from equilibrium to steady-state transport properties begs the question about transient dynamics: what happens if such a slowly relaxing liquid is suddenly subjected to shear, regarding its dynamical correlations as the system progresses from equilibrium towards its steady state? One can investigate these effects most easily by looking at the waiting-time dependent dynamical two-time correlation functions: switching on the external shear flow at  $t = 0$ , one measures the correlations of dynamical variables between some waiting time  $t_w > 0$ , and a correlation time  $t = t_w + \tau > t_w$ . Of particular interest are the so-called transient correlation

functions, obtained for  $t_w = 0$ , to be compared with the reference cases of equilibrium and steady state.

In the present contribution, we address this issue by presenting an approximate relationship between these three relevant types of dynamical two-point correlation functions.

Recently, the dynamical evolution after switching on shear flow of steady rate  $\dot{\gamma}$  has been addressed [1] by a combination of techniques: theoretically, in the framework of mode-coupling theory (MCT) for colloidal rheology and an integration-through transients (ITT) approach, experimentally, using confocal microscopy, and with computer simulation of a damped Newtonian-dynamics model. All three methods yield a consistent picture: a shear stress  $\sigma(t)$  builds up at  $t > 0$  after switch-on, but does not grow monotonically towards its steady-state value  $\sigma_\infty$ . It rather exhibits an intermediate “overshoot” at times corresponding to an overall strain  $\gamma = \dot{\gamma}t \approx 0.1$ . Such stress overshoot phenomena are in fact well-known [2–4], but despite their ubiquity, their microscopic origin, in particular for the fully homogeneous flow profiles studied, remains somewhat vague. In Ref. [1], simulations were able to connect it to a sudden change in the mean-squared displacement (MSD) of a tracer particle: even for the directions perpendicular to the shear flow where no explicit advection occurs, one observes a super-diffusive regime as the transient MSD,  $\delta r^2(t, t_w = 0)$ , leaves the equilibrium curve around  $\gamma \approx 0.1$ , to cross over to the (much larger) steady-state curve which it reaches at  $\gamma \approx 1$ . In this regime, MD simulations found motion to be almost ballistic,  $\delta r^2(t \approx 0.1/\dot{\gamma}, 0) \approx t^x$  with  $x \approx 2$ . In experiment

(closer to Brownian dynamics), this superdiffusion was not as pronounced, yielding  $x$  only slightly larger than 1. Within MCT-ITT and an additional ad-hoc approximation akin to a generalized Stokes-Einstein relation, it could be shown that the stress overshoot and superdiffusion are directly connected and originate from an overrelation of microscopic stresses: the transient stress autocorrelation function (called a dynamical shear modulus) does not decay monotonically to zero, but exhibits a “dip” in the corresponding strain regime where it becomes slightly negative just before reaching its zero long-time limit.

Thus, the details on the evolution from equilibrium dynamics to far-from-equilibrium dynamics under shear are encoded in transient correlation functions. This raises a two-fold interest in these transient correlation functions: first, given information on both equilibrium and the steady state, what can one infer about the transient dynamics? Second, recalling that MCT and ITT generically build upon the transient correlation functions, can one test their generic implications?

The relationship among the various two-point dynamical correlation functions that we present in the following, builds upon the ITT formalism, without explicit reference to MCT. It should thus hold quite generally, at least qualitatively. We demonstrate this by comparing with computer-simulation data for both a Brownian and a non-Brownian system. For dense liquids and colloidal suspensions in equilibrium, it is a well-tested paradigm, that the long-time behavior of the correlation functions does not (up to an overall time unit) depend on the type of short-time motion, be it ballistic (Newtonian dynamics) or diffusive (Brownian colloidal particles). This in fact defines the regime of quiescent “structural relaxation”, where slow relaxation processes arising from collective caging of particles govern the dynamics of the system.

This equivalence of Newtonian and Brownian systems does not need to hold far from equilibrium, although similar shear-thinning effects are seen both in colloidal suspensions and atomistic metallic melts. Indeed, differences were observed regarding the extent of superdiffusive motion in the transient MSD [1]. Note that in the MD simulations of Ref. [1], shear was implemented through the boundaries of the (periodically repeated) simulation box only, by Lees-Edwards boundary conditions. Hence, particles at the center of the box remain at rest also for a short time after switching on the flow, until a linear shear profile propagates from the boundaries towards the center. It was argued that this time scale is short compared to the  $\dot{\gamma}t \approx 0.1$  of interest. In Brownian dynamics, the issue can be set aside, as there one immediately modifies the solvent flow profile throughout the box when implementing shear (in addition to Lees-Edwards boundary conditions). This situation also being closer to what MCT-ITT models, is another motivation to complement the MD simulation data already partially discussed in Ref. [1] with new simulations incorporating diffusive

short-time motion.

The peculiar features of the transient correlation functions not only highlight possible differences in the non-equilibrium response of the different system types. They also provide direct tests of the MCT-ITT formalism. At the core of ITT is a reformulation of non-equilibrium averages in terms of history integrals over equilibrium averages where the full nonequilibrium time-dependence is kept in the evolution of the dynamical variables. In the case of steady shear, this is precisely the transient correlation function measurable in experiment or simulation where a shear flow is switched on immediately at  $t = 0$ .

While the transient ( $t_w = 0$ ) correlation function is the natural object to be treated in MCT-ITT, steady-state and more generally  $t_w$ -dependent correlation functions have, in this approach, to be calculated afterwards. Our main result here enables MCT-ITT to do just that: by obtaining equilibrium and transient correlation functions from any theory, correlators for all  $t_w$  can be expressed.

The paper is structured as follows: after some notational clarification (Sec. II), we present in Sec. III the main theoretical derivation of our formulas. Section IV is devoted to a schematic-MCT illustration of the results, while Sec. V presents the analysis of computer-simulation data. Section VI concludes the discussion.

## II. CORRELATION FUNCTIONS

Given two dynamical fluctuating variables  $\delta f$  and  $\delta g$ , i.e., functions with zero average that depend on the state-point  $\Gamma$  of the system, one defines the two-point correlation function  $C^{fg}(t, t_w)$  for  $t \geq t_w$  [5],

$$C^{fg}(t, t_w) = \iint d\Gamma d\Gamma' \delta g(\Gamma) P(\Gamma, t | \Gamma', t_w) \times \delta f^*(\Gamma') \Psi_{t_w}(\Gamma'). \quad (1)$$

Here,  $P(\Gamma, t | \Gamma', t_w)$  denotes the conditional probability that the system resides at state point  $\Gamma$  at time  $t = t_w + \tau$ , given it was at state point  $\Gamma'$  at time  $t_w$ .  $\Psi_{t_w}(\Gamma')$  is the probability that the system is at  $\Gamma'$  at time  $t_w$ , and of course just the (nonequilibrium) distribution function. The latter is assumed to be equal to the equilibrium distribution for times  $t < 0$ ,  $\Psi_{t < 0}(\Gamma) = \Psi_e(\Gamma)$ , and to asymptotically reach a time-independent steady state for long times,  $\Psi_{t \rightarrow \infty}(\Gamma) = \Psi_s(\Gamma)$ . These reference limits define the equilibrium and steady-state ensemble averages,

$$\langle \dots \rangle = \int d\Gamma \Psi_e(\Gamma) \dots, \quad (2a)$$

$$\langle \dots \rangle^{(\dot{\gamma})} = \int d\Gamma \Psi_s(\Gamma) \dots. \quad (2b)$$

The conditional probability  $P$  in Eq. (1) encodes the dynamics of the system, subject to the external field. We will use the following property [5]: for the case of switching on a constant shear flow,  $P(\Gamma, t_w + \tau | \Gamma', t_w)$  becomes

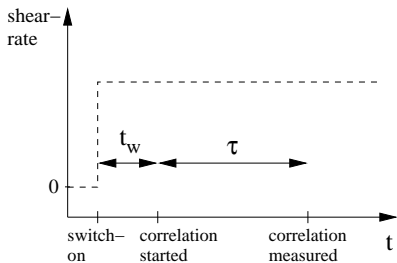


FIG. 1: Schematic representation of the times appearing in the two-point correlation functions, Eq. (1): waiting time  $t_w > 0$ , measurement time  $t$ , and correlation time  $\tau = t - t_w > 0$ .  $t = 0$  corresponds to the time where homogeneous, linear shear flow is instantaneously switched on.

independent on  $t_w$  for all  $t_w > 0$ . For Brownian dynamics, this means that both  $\Psi_{t_w}$  and  $P$  obey the same differential (Smoluchowski) equation, i.e., the underlying stochastic process is assumed to have a Markovian property [6]. As long as  $\Psi_{t_w}(\Gamma')$  evolves, the correlation function  $C^{fg}(t, t_w)$  will depend on its two time arguments separately; we will generally call these functions “waiting-time dependent” (for waiting time  $t_w$ ). When it is clear from the context, we omit the superscript denoting the variables and abbreviate  $C_{t_w}(\tau) \equiv C(t_w + \tau, t_w)$ . While potentially interesting, we ignore correlation functions formed with  $t_w < 0$  and  $t > 0$ . Figure 1 schematically summarizes the sequence of correlation and measurement times.

As  $t_w \rightarrow \infty$ , the steady-state correlation function is approached, which we denote by  $C_\infty(\tau) \equiv C(t, +\infty)$ . Correspondingly, as  $t_w < -\tau$ , one obtains the equilibrium correlation function,  $C_e(\tau) \equiv C(t, -\infty)$ . Both  $C_\infty(\tau)$  and  $C_e(\tau)$  are functions of the time difference  $\tau$  only. Among the general waiting-time dependent correlation functions, a particular role is played by the  $t_w = 0$  case: recalling  $\Psi_0 = \Psi_e$ , we recognize the so-called transient correlation function  $C_0(\tau) \equiv C(t, 0)$ , where the time evolution as determined by the transition rates  $P$  is the nonequilibrium one, but averaging is performed with the equilibrium distribution.

Note that we do not in general assume  $C_e(\tau)$  to decay to zero for  $\tau \rightarrow \infty$ : in (idealized) glass states, it attains a finite positive long-time limit, called the nonergodicity factor or glass form factor [7].

In comparing with computer simulations, we set for simplicity  $f = g$  to be the one-particle microscopic number density,  $\delta f = \exp[i\mathbf{q} \cdot \mathbf{r}_s]$  with wave vector  $\mathbf{q}$  and the position of the singled-out particle  $\mathbf{r}_s$ . To further simplify the discussion, we restrict ourselves to wave vectors perpendicular to the flow direction. This obliterates the need of introducing wave-vector advection in order to account for the affine motion imposed by the shear [8].

Connected to the zero-wavevector limit of tagged-particle density fluctuations is of course the mean-

squared displacement (MSD),

$$\delta r^2(t, t_w) = \iint d\Gamma d\Gamma' [\mathbf{r}_s(\Gamma) - \mathbf{r}_s(\Gamma')]^2 \times P(\Gamma, t | \Gamma', t_w) \Psi_{t_w}(\Gamma'), \quad (3)$$

also schematically written as  $\delta r^2(t, t_w) = \langle [\mathbf{r}_s(t) - \mathbf{r}_s(t_w)]^2 \rangle^{si}$  where  $\langle \dots \rangle^{si}$  denotes averaging over particles and runs as done in a simulation. Again, the MSD comes in its equilibrium ( $\delta r_e^2(\tau)$ ), steady-state ( $\delta r_\infty^2(\tau)$ ), and transient ( $\delta r_0^2(\tau)$ ) varieties.

We generally consider a system of  $N$  spherical particles without internal degrees of freedom, enclosed in a volume  $V$ . Choosing units, we set the thermal energy  $k_B T = 1$  throughout. For the stochastic-dynamics simulations as well as the theory, we assume diffusive short-time motion governed by a bare diffusion coefficient  $D_0 = 1$ ; we do not take into account explicit solvent or hydrodynamic interactions among the particles. A typical interaction diameter of the particles,  $\sigma = 1$ , sets the unit length.

We choose coordinates such that the external flow acts in the Cartesian  $x$ -direction (called flow direction), and varies along  $y$  (called gradient direction). In 3D, the system is invariant along the  $z$ -axis (neutral direction). Thus, the velocity field induced by the shear can be written as  $\mathbf{v}(\mathbf{r}) = \dot{\gamma} y \hat{\mathbf{x}}$  with the velocity-gradient tensor  $\boldsymbol{\kappa} = \dot{\gamma} \hat{\mathbf{x}} \hat{\mathbf{y}}$ , where  $\hat{\mathbf{x}}$  is a unit vector in the direction of  $\mathbf{x}$ .

### III. MICROSCOPIC THEORY

Within the ITT formalism, we now derive expressions for the time-dependent correlation functions of interest. We begin by recalling the exact starting points of ITT, before introducing approximations that lead to our final result, presented in Sec. III C.

#### A. Integration Through Transients

For the theoretical derivation, assume interaction forces among the particles to be  $\mathbf{F}_i = -\partial_i U$  ( $i = 1, \dots, N$ ), where  $U$  is the total potential energy of the system. In the thermodynamic limit, the particle distribution function  $\Psi_t(\Gamma)$  of the Brownian system subject to homogeneous shear flow described by the velocity-gradient tensor  $\boldsymbol{\kappa}(t)$ , is then taken to obey the Smoluchowski equation [9, 10],

$$\partial_t \Psi_t(\Gamma) = \Omega(t) \Psi_t(\Gamma), \quad (4a)$$

$$\Omega(t) = \Omega_e + \delta\Omega(t) = \sum_i \partial_i \cdot [\partial_i - \mathbf{F}_i - \boldsymbol{\kappa}(t) \cdot \mathbf{r}_i]. \quad (4b)$$

Here,  $\Omega$  is the Smoluchowski operator (SO), consisting of the equilibrium (quiescent) contribution,  $\Omega_e = \sum_i \partial_i \cdot [\partial_i - \mathbf{F}_i]$ , and the nonequilibrium term representing homogeneous driving. For the case considered here

(switching on constant shear flow of rate  $\dot{\gamma}$  at  $t = 0$ ),  $\delta\Omega(t) = \delta\Omega = -\sum_i \partial_i \cdot \boldsymbol{\kappa} \cdot \mathbf{r}_i$  independent on  $t$  for  $t > 0$  and zero else. Hence,

$$\Omega(t) = \begin{cases} \Omega_e & \text{for } t < 0, \\ \Omega^{(\dot{\gamma})} & \text{for } t > 0, \end{cases} \quad (5)$$

where  $\Omega^{(\dot{\gamma})}$  does not depend on time. The equilibrium distribution function  $\Psi_e$  is the stationary solution of Eq. (4) without shear,  $\Omega_e \Psi_e \equiv 0$ , viz.  $\Psi_e \propto \exp(-U/k_B T)$ . Including shear,  $\Omega^{(\dot{\gamma})} \Psi_s \equiv 0$  defines the steady-state distribution. In this stationary state, the distribution function is time-shift invariant as in equilibrium, but the system is not in thermal equilibrium due to a non-vanishing probability current [11].

The integration through transients (ITT) formalism allows to reformulate the nonequilibrium averages formed with the (unknown)  $t_w$ -dependent distribution  $\Psi_{t_w}$  in terms of equilibrium averages. Formally solving the Smoluchowski equation, Eq. (4), as an integral equation with the boundary condition  $\Psi(t=0) = \Psi_e$ , one gets for  $t_w \geq 0$ ,

$$\Psi(t_w) = e^{\Omega^{(\dot{\gamma})} t_w} \Psi_e = \Psi_e + \int_0^{t_w} ds \Omega^{(\dot{\gamma})} e^{\Omega^{(\dot{\gamma})} s} \Psi_e. \quad (6)$$

Recalling  $\Omega^{(\dot{\gamma})} \Psi_e = \delta\Omega \Psi_e = \sigma_{xy} \Psi_e$  [10], integration by parts yields

$$\int d\Gamma \Psi_{t_w} \dots = \int d\Gamma \Psi_e \left[ 1 + \dot{\gamma} \int_0^{t_w} ds \sigma_{xy} e^{\Omega^\dagger s} \right] \dots \quad (7)$$

with the microscopic (potential) stress tensor element  $\sigma_{xy} = -\sum_i F_i^x y_i$  [10]. Here,  $\Omega^\dagger = \sum_i [\partial_i + \mathbf{F}_i + \mathbf{r}_i \cdot \boldsymbol{\kappa}^T] \cdot \partial_i$  is the operator adjoint to  $\Omega^{(\dot{\gamma})}$ . With  $t_w \rightarrow \infty$ , the steady-state average in Eq. (2) immediately follows

$$\langle \dots \rangle^{(\dot{\gamma})} = \langle \dots \rangle + \dot{\gamma} \int_0^\infty ds \langle \sigma_{xy} e^{\Omega^\dagger s} \dots \rangle. \quad (8)$$

The Smoluchowski equation, Eq. (4), is also taken to determine the conditional probability  $P$  appearing in Eq. (1), and thus [5, 10], for  $t_w > 0$ ,  $P(\Gamma, t_w + \tau | \Gamma', t_w) = \exp[\Omega^{(\dot{\gamma})} \tau] \delta(\Gamma - \Gamma')$ . Rewriting in terms of the adjoint operator, this gives

$$C_\infty^{fg}(\tau) = \langle \delta f^* e^{\Omega^\dagger \tau} \delta g \rangle^{(\dot{\gamma})} \quad (9a)$$

and, for the transient correlation function,

$$C_0^{fg}(\tau) = \langle \delta f^* e^{\Omega^\dagger \tau} \delta g \rangle. \quad (9b)$$

Note its distinction from the equilibrium correlation function, where the equilibrium adjoint SO,  $\Omega_e^\dagger$ , appears,

$$C_e^{fg}(\tau) = \langle \delta f^* e^{\Omega_e^\dagger \tau} \delta g \rangle. \quad (9c)$$

For the general two-time correlation function at finite  $t_w > 0$ , inserting into Eq. (7) gives

$$C_{t_w}^{fg}(\tau) = C_0^{fg}(\tau) + \dot{\gamma} \int_0^{t_w} ds \langle \sigma_{xy} e^{\Omega^\dagger s} \delta f^* e^{\Omega^\dagger \tau} \delta g \rangle. \quad (10)$$

This equation is formally exact, although the evaluation of the dynamical three-point average in the integral will generally be hard. We are therefore forced to introduce approximations at this point.

## B. Approximations for Correlation Functions

To simplify the discussion, we now restrict ourselves to auto-correlation functions ( $\delta f = \delta g$ ) of dynamical fluctuations without explicit shear-advection,  $\delta f \equiv f(\{y_i, z_i\})$ . Similar results can be expected for correlation functions involving shear-advection quantities (i.e., dynamical variables explicitly depending also on positions  $x_i$  along the shear flow), but one then has to be careful in first extracting the affine transformations induced by the steady shear.

To obtain a tractable expression for the general  $t_w$ -dependent correlation function, let us apply a familiar identity in the Zwanzig-Mori operator formalism (cf. Eq. (11) in Ref. [12] and also Ref. [13]): introducing a projector onto  $\delta f$ ,  $\mathcal{P}_f = \delta f \langle \delta f^* \delta f \rangle^{-1} \langle \delta f^* \cdot$ , with complement  $\mathcal{Q}_f = 1 - \mathcal{P}_f$ , we get from Eq. (10),

$$C_{t_w}^f(\tau) = C_0^f(\tau) \left[ 1 + \dot{\gamma} \int_0^{t_w} ds \frac{\langle \sigma_{xy} e^{\Omega^\dagger s} \delta f^* \delta f \rangle}{\langle \delta f^* \delta f \rangle} \right] + \dot{\gamma} \int_0^\tau d\tau' \int_0^{t_w} ds \frac{\langle \sigma_{xy} e^{\Omega^\dagger s} \delta f^* \mathcal{U}(\tau - \tau') \delta f \rangle}{\langle \delta f^* \delta f \rangle} C_0^f(\tau'), \quad (11)$$

with the restricted time evolution operator

$$\mathcal{U}(a) = \mathcal{Q}_f \exp[\mathcal{Q}_f \Omega^\dagger \mathcal{Q}_f a] \mathcal{Q}_f \Omega^\dagger. \quad (12)$$

We thus identify two contributions to the difference between the nonequilibrium waiting-time dependent correlator and the transient one. The first is a  $\tau$ -independent renormalization of the equal-time value and corresponds, e.g., to the difference of distorted and equilibrium static structure factor if  $t_w \rightarrow \infty$  [8, 14]. Note that in Ref. [8], only this term for the difference of the correlators is considered. It vanishes for tagged-particle density fluctuations, since with  $\delta f = \exp[i\mathbf{q} \cdot \mathbf{r}_s]$ , the average of  $\delta f^* \delta f$  is unity in any ensemble.

The second term contains a more complicated dependence on both  $t_w$  and  $\tau$ , and cannot easily be evaluated. But one recognizes that inserting a projector onto  $\sigma_{xy}$  before the  $\delta f^*$  term allows to factorize the integral according to the different time dependences. The right-hand part containing  $\mathcal{U}(\tau - \tau')$  then becomes proportional to  $\langle \sigma_{xy} \delta f^* \mathcal{U}(\tau - \tau') \delta f \rangle$ , for which the operator



identity that led to Eq. (11) can be rolled back by noting  $\langle \sigma_{xy} \delta f^* \delta f \rangle = 0$  due to symmetry ( $\delta f^* \delta f$  is symmetric in coordinates  $x$  and  $y$ , while  $\sigma_{xy}$  is antisymmetric). Thus, assuming the dominant part of the last integral in Eq. (11) to be given by the projection of  $\delta f$  onto  $\sigma_{xy}$ , we get

$$C_{t_w}^f(\tau) \approx \alpha_f(t_w) C_0^f(\tau) + \dot{\gamma} \tilde{\sigma}(t_w) \langle \sigma_{xy} \delta f^* e^{\Omega^\dagger \tau} \delta f \rangle, \quad (13)$$

where we have abbreviated the static renormalization by  $\alpha_f(t_w) = 1 + \dot{\gamma} \int_0^{t_w} ds \langle \sigma_{xy} \exp[\Omega^\dagger s] \delta f^* \delta f \rangle / \langle \delta f^* \delta f \rangle$ . In Refs. [11, 15] the simplified version with  $\alpha_f(t_w) = 1$  was considered which, again, holds exactly for tagged particle dynamics.

Note that formally, we had to introduce a projector  $\mathcal{P}_\sigma = \sigma_{xy} \langle \sigma_{xy} \sigma_{xy} \rangle^{-1} \langle \sigma_{xy}$  that is ill-defined for the case of hard spheres, as there, the instantaneous shear modulus  $\langle \sigma_{xy} \sigma_{xy} \rangle$  diverges [16, 17]. However, we only require

$$\tilde{\sigma}(t_w) = \int_0^{t_w} \frac{\langle \sigma_{xy} e^{\Omega^\dagger s} \sigma_{xy} \rangle}{\langle \sigma_{xy} \sigma_{xy} \rangle} ds, \quad (14)$$

i.e., the integrated normalized shear modulus [10, 18–21], to exist. We assume that this integral can be regularized for hard spheres, as outlined in Appendix A.

The remaining correlation function in Eq. (13) is nothing but the *waiting-time derivative* of  $C_{t_w}^f(\tau)$  at  $t_w = 0$  [11], as is immediately clear from taking the  $t_w$ -derivative on both sides of Eq. (10),

$$\dot{\gamma} \langle \sigma_{xy} \delta f^* e^{\Omega^\dagger \tau} \delta f \rangle = \left. \frac{\partial}{\partial t_w} C_{t_w}^f(\tau) \right|_{t_w=0}. \quad (15)$$

It describes the initial change of the two-time correlator with  $t_w$  at fixed correlation-time window  $\tau$ . Our approximation then reads

$$C_{t_w}^f(\tau) \approx \alpha_f(t_w) C_0^f(\tau) + \tilde{\sigma}(t_w) \left. \frac{\partial}{\partial t_w} C_{t_w}^f(\tau) \right|_{t_w=0}, \quad (16)$$

and Eq. (13) can be interpreted as “coupling at  $t_w \rightarrow 0$ ”, incorporating the exact result to first order in  $t_w$ : recalling  $\tilde{\sigma}(t_w) = t_w + \mathcal{O}(t_w^2)$  and  $\alpha(t_w) = 1 + \mathcal{O}(t_w^2)$ ,

$$C_{t_w}^f(\tau) = C_0^f(\tau) + \left. \frac{\partial}{\partial t_w} C_{t_w}^f(\tau) \right|_{t_w=0} t_w + \mathcal{O}((\dot{\gamma} t_w)^2). \quad (17)$$

Equation (13) extends this identity to finite  $t_w$  by accounting for the static change  $\alpha_f(t_w)$  exactly (in principle), and relating the further  $t_w$  dependence to the integrated shear modulus  $\tilde{\sigma}$ .

We still have to close this approximation by relating the waiting-time derivative to known correlation functions. As was shown in Refs. [11, 15], one can, using integration by parts and the identity  $\delta \Omega^\dagger \delta f = 0$ , arrive

at

$$\left. \frac{\partial}{\partial t_w} C_{t_w}^f(\tau) \right|_{t_w=0} = \langle \delta f^* \delta \Omega^\dagger e^{\Omega^\dagger \tau} \delta f \rangle = \frac{\partial}{\partial \tau} C_0^f(\tau) - \langle \delta f^* \Omega_e^\dagger e^{\Omega_e^\dagger \tau} \delta f \rangle. \quad (18)$$

This equation highlights the connection of the waiting-time derivative to time derivatives of correlation functions: the derivative of the transient correlator  $C_0^f(\tau)$  has two parts, one containing the equilibrium operator  $\Omega_e^\dagger$ , and one containing the nonequilibrium shear-induced  $\delta \Omega^\dagger$ . The former term corresponds to the short-time dynamics of the correlation function, unaffected by shear as long as  $Pe_0 \ll 1$ , while the latter term, the waiting-time derivative, is governed by the shear-induced decay of the correlator at long times.

The equilibrium derivative  $\Omega_e^\dagger \delta f^*$  in the last term of Eq. (18) de-correlates quickly as the particles lose memory of their initial motion even without shear. In this case, the latter term is the time derivative of the equilibrium correlator,  $C_e^f(\tau)$ . A shear flow switched on at  $\tau = 0$  will generally lead to even faster decorrelation, prompting us to approximate  $e^{\Omega^\dagger \tau} \approx e^{\Omega_e^\dagger \tau} \mathcal{P}_f e^{-\Omega_e^\dagger \tau} e^{\Omega^\dagger \tau}$ . This approximation used in the last term in Eq. (18) as well as in  $C_0^f(\tau)$  leads to

$$\frac{\langle \delta f^* \Omega_e^\dagger \exp[\Omega^\dagger \tau] \delta f \rangle}{\langle \delta f^* \exp[\Omega^\dagger \tau] \delta f \rangle} \approx \frac{\langle \delta f^* \Omega_e^\dagger \exp[\Omega_e^\dagger \tau] \delta f \rangle}{\langle \delta f^* \exp[\Omega_e^\dagger \tau] \delta f \rangle} \quad (19)$$

and thus

$$\langle \delta f^* \Omega_e^\dagger e^{\Omega^\dagger \tau} \delta f \rangle \approx \frac{C_0^f(\tau)}{C_e^f(\tau)} \frac{\partial}{\partial \tau} C_e^f(\tau). \quad (20)$$

Inserting this approximation in Eq. (18) yields [11]

$$\left. \frac{\partial}{\partial t_w} C_{t_w}^f(\tau) \right|_{t_w=0} \approx \frac{\partial}{\partial \tau} C_0^f(\tau) - \frac{C_0^f(\tau)}{C_e^f(\tau)} \frac{\partial}{\partial \tau} C_e^f(\tau). \quad (21)$$

The two terms in this equation have an intuitive interpretation: if  $\dot{\gamma} \tau \ll 1$ , there holds  $C_0^f(\tau) = C_e^f(\tau) + \mathcal{O}(\dot{\gamma} \tau)$  [17], and the right hand side of Eq. (21) cancels in leading order in  $\dot{\gamma} \tau$ . This is expected on physical grounds, since the short-time decay of the correlation function is independent of  $t_w$  at least for small  $t_w$ . For  $\tau = 0$ , Eq. (21) yields zero exactly, in agreement with Eq. (15), where  $\langle \sigma_{xy} \delta f^* \delta f \rangle = 0$  due to symmetry. On the other hand, for  $\dot{\gamma} \tau = \mathcal{O}(1)$  with  $Pe \gg 1$  (i.e., the relaxation time of  $C_e(\tau)$  is much larger than the shear-induced relaxation time  $\mathcal{O}(1/\dot{\gamma})$ ), the last term in Eq. (21) vanishes, and the waiting-time derivative is given by the time derivative of the transient correlator. We thus refer to the term on the left hand side and the last term in Eq. (21) as *long-time* and *short-time* derivatives, respectively.

The approximation leading to Eq. (21) can further be made plausible by considering states that are glassy in

the quiescent equilibrium; setting the second term on the right-hand side to zero, and writing out the derivatives, one gets

$$C_{\delta t}^f(\tau) \approx C_0^f(\tau + \delta t), \quad \tau \rightarrow \infty, \quad (22)$$

for small  $\delta t$ . This embodies the physical argument that at large times, whenever the equilibrium dynamics is frozen and the transient correlator is on the plateau, shear effects set in as function of  $t$  rather than  $\tau$ .

### C. Relation for the Two-Time Correlator

Equations (21) and (16) taken together yield an approximation that allows us to study the waiting-time dependence of the non-equilibrium two-time correlation function,

$$C_{t_w}^f(\tau) \approx C_0^f(\tau) \left[ \alpha_f(t_w) + \tilde{\sigma}(t_w) \frac{d}{d\tau} \left( \ln |C_0^f(\tau)| - \ln |C_e^f(\tau)| \right) \right] \quad (23)$$

A brief discussion of this result might be in order. First, we recognize that for weak shear,  $Pe \ll 1$ , the second term in Eq. (23) does not contribute, as in this regime  $C_0^f(\tau) \approx C_e^f(\tau)$ , and hence the normalized waiting-time dependent correlation function likewise does not change. This ensures that we correctly recover linear response. On the other hand, for  $Pe \gg 1$ , the derivative of the transient correlation function will dominate the second term in the equation.

Let us also note the equivalent approximation to Eq. (23) for the mean-squared displacement, easily derived from the  $q \rightarrow 0$  limit of the corresponding tagged-particle density correlation function. Considering the  $y$ - or  $z$ -direction for simplicity,

$$\delta z^2(\tau) = \lim_{q \rightarrow 0} \frac{1 - C^f(\tau)}{q^2}, \quad (24)$$

where  $\delta f = \exp[iqz_s]$  with  $z_s$  the  $z$ -coordinate of the tagged particle. Performing the  $q \rightarrow 0$  limit in Eq. (23) directly yields (recall that  $\alpha_f(t_w) \equiv 1$  for tagged-particle density fluctuations)

$$\delta z_{t_w}^2(\tau) \approx \delta z_0^2(\tau) + \tilde{\sigma}(t_w) \frac{d}{d\tau} (\delta z_0^2(\tau) - \delta z_e^2(\tau)). \quad (25)$$

Considering only directions perpendicular to the shear direction, the MSD is linear in time for long times, i.e.,  $\delta z^2(\tau) \sim \tau$  as  $\tau \rightarrow \infty$ . If  $\dot{\gamma}\tau \gg 1$  (and thus  $\dot{\gamma}t \gg 1$ ), it is plausible that the transient MSD describes the same diffusivity as the stationary one, and the time-derivatives of the two functions have to be equal in that limit, as reproduced by Eq. (25).

Equations (23) and (25) constitute our main theoretical result: calculating, e.g.,  $C_0^f(\tau)$  and  $C_e^f(\tau)$  within

MCT, the above equations give access to the general waiting-time dependent  $C_{t_w}^f(\tau)$ , including the steady-state correlation function usually measured in experiments.

The equations can also be rewritten in order to determine the transient correlation function from the more commonplace equilibrium and steady-state ones. To this end, note that Eq. (23) is solved by

$$C_0^f(\tau) = e^{-\alpha_f(t_w)\tau/\tilde{\sigma}(t_w)} C_e^f(\tau) + C_e^f(\tau) \int_0^\tau \frac{e^{-\alpha_f(t_w)(\tau-s)/\tilde{\sigma}(t_w)} C_{t_w}^f(s)}{\tilde{\sigma}(t_w) C_e^f(s)} ds. \quad (26)$$

Taking  $t_w \rightarrow \infty$  yields an expression determining the transient correlator  $C_0^f(\tau)$  in terms of both the equilibrium one,  $C_e^f(\tau)$ , and the stationary one,  $C_\infty^f(\tau)$ . For small waiting times,  $\tilde{\sigma}(t_w) = t_w + \mathcal{O}(t_w^2)$  can be used, and for tagged-particle correlation functions where  $\alpha_f(t_w) = 1$ , no unknown parameters remain in Eq. (26). For the mean-squared displacement, a similar transform holds,

$$\delta z_0^2(\tau) = \delta z_e^2(\tau) + \int_0^\tau e^{-(\tau-s)/\tilde{\sigma}(t_w)} \frac{\delta z_{t_w}^2(s) - \delta z_e^2(s)}{\tilde{\sigma}(t_w)} ds. \quad (27)$$

Incidentally, these forms are also, for direct testing with computer-simulation data, more stable numerically than Eqs. (23) and (25) as they do not involve time-derivatives. We will therefore use them primarily in Sec. V where we use  $C_e^f(\tau)$  and  $C_{t_w}^f(\tau)$  taken from computer-simulation data to assess the quality of the approximation by comparing the calculated and simulated  $C_0^f(\tau)$ .

## IV. A SCHEMATIC MCT MODEL

Equations (23) and (25) represent the central theoretical result of our paper. In this section, we visualize their physical content by choosing a simple toy model for calculating the transient two-time correlation functions. For the purpose of our discussion, it is easiest to choose a schematic model of mode-coupling theory, as these models are very successful both in analyzing real-world data and for understanding the generic features of colloidal systems under shear.

### A. Schematic Equations

Let us consider a single, normalized transient correlation function  $C_0(\tau) = \phi(\tau)$ , to represent the collective density-fluctuation correlators for some dominant (nearest-neighbor) length scale. Recently, a schematic model allowing to treat arbitrarily time-dependent flow

has been proposed [22], whose equations of motion in the case of steady simple shear reduce to

$$0 = \tau_0 \partial_\tau \phi(\tau) + \phi(\tau) + \int_0^\tau d\tau' m(\tau, \tau - \tau') \partial_{\tau'} \phi(\tau') d\tau', \quad (28a)$$

$$m(a, b) = h_1(a) h_2(b) \hat{m}(b), \quad (28b)$$

$$\hat{m}(a) = [v_1 \phi(a) + v_2 \phi(a)^2], \quad (28c)$$

$$h_{1,2}(a) = 1 / [1 + (\dot{\gamma} a / \gamma_c)^2]. \quad (28d)$$

Here, the  $h_i(a)$  are *ad-hoc* forms for the strain-induced reduction of the memory kernel, inspired by the appearance of similarly time dependent terms in the original MCT vertices due to wave-vector advection. Its precise form is not crucial, and we follow the choice of Ref. [22] by choosing a simple decaying function that is even in the strain. There,  $\gamma_c = 0.1$  was introduced to model the typical cage-breaking length scale: strains of about 10% mark the point where noticeable strain reduction of memory effects sets in.  $1/\tau_0$  is an initial decay rate that serves to set the unit of time.

For  $\dot{\gamma} \equiv 0$ , Eqs. (28) reduce to the well-known  $F_{12}$  model of quiescent MCT [23], whose solutions provide the equilibrium correlator  $\phi_e(\tau)$ . Setting  $h_1 \equiv 1$  further reduces our model to the  $F_{12}^{(\dot{\gamma})}$  model [17], originally proposed for the analysis of steady shear flows. This model provides excellent fits to the flow curves from large scale simulations [24], and the extension setting  $h_1 \equiv h_2$  does not qualitatively change these flow curves, while keeping a closer connection to the more general time-dependent flows [22].

The  $F_{12}$  model has glass transitions along a line of coupling parameters  $(v_1^c, v_2^c)$ , where the long time limit  $f = \lim_{\tau \rightarrow \infty} \phi_e(\tau)$  jumps discontinuously from zero to its critical value  $f^c$ . The choice  $v_2^c = 2$  is known to yield good agreement with the asymptotic features expected for the hard-sphere glass transition; it implies  $v_1^c = 2(\sqrt{2} - 1)$ . The separation parameter  $\varepsilon$  then serves to quantify the distance to the transition: we set  $(v_1, v_2) = (v_1^c, v_2^c)(1 + \varepsilon)$  such that  $\varepsilon > 0$  indicates glassy states,  $\varepsilon < 0$  fluid ones.

In order to evaluate Eq. (23), we further need a schematic-model version of Eq. (14) yielding  $\tilde{\sigma}(t_w)$ . We let [11, 15]

$$\tilde{\sigma}(t_w) = \frac{\dot{\gamma}}{3} \int_0^{t_w} \phi(s) ds, \quad (29)$$

which can be regarded as a schematic version of the generalized Green-Kubo relation derived within ITT and the MCT approximation [22], where we approximate the dynamical shear modulus  $G(s) \approx \phi(s)/3$ , a reasonable approximation in particular at long times. The factor  $1/3$  accounts for the fact that the plateau in the shear modulus is empirically found to be smaller than that of the correlator. In fact, Eq. (29) neglects prefactors and an anisotropic wave-vector integral that appears in the microscopic Green-Kubo relation; this means also that we

have lost the correct description of the stress overshoot. To include this effect, one would need to evaluate Eq. (29) microscopically, as done e.g. in Ref. [1]. Eq. (29) is thus to be regarded merely as a plausible closure that incorporates the structure of MCT-ITT that  $\tilde{\sigma}(t_w)$  is dominated by an integral over the density correlation functions, effectively cut off by the slow relaxation time of those correlators.

Equations analogous to Eqs. (28) hold for the schematic transient tagged-particle correlation function  $\phi^s(\tau)$ ; the only difference is in the precise form of the mode-coupling kernel  $\hat{m}^s(a)$ , Eq. (28c). Its microscopic expression for tagged-particle density fluctuations can be worked out [25], and will be discussed elsewhere. For our purpose, we copy the form of the well-known schematic quiescent tagged-particle model, the so-called Sjögren model,  $\hat{m}^s(a) = v_s \phi(a) \phi^s(a)$ . Here, a coupling coefficient  $v_s > 0$  appears that describes the strength of the tagged-particle coupling to the collective density fluctuations. This parameter plays no qualitative role in the further discussion; we fix it to  $v_s = 5$ .

The transient MSD (in the neutral or gradient direction) is the solution of a similar memory equation, cf. Refs. [1, 26],

$$\tau_0 \delta \bar{z}_0^2(\tau) + \int_0^\tau \bar{m}^s(\tau - \tau') \delta \bar{z}_0^2(\tau') d\tau' = 2\tau, \quad (30)$$

where we denote the schematic-model transient MSD by  $\delta \bar{z}_0^2$  in order to avoid confusion with its microscopic counterpart. In principle, its memory kernel will not be identical to the one appearing in the tagged-particle-correlator equation, but the MCT approximation for the self-density fluctuations imply that both these memory kernels are bilinear functionals of  $\phi$  and  $\phi^s$ , so that they can be approximated as equal on the schematic level. Note however that  $\bar{m}^s$  must be a single-time function, as is found in the full microscopic derivation [25], in order to recover long-time diffusion. We therefore set  $\bar{m}^s(a) = h_2(a) \hat{m}^s(a)$ .

## B. Results of the Schematic Model

We now turn to a discussion of the central Eqs. (23) and (25) with the aid of the schematic transient and equilibrium correlators and MSD defined in the previous section. In order to highlight the non-trivial effect of the waiting time, we set  $\alpha \equiv 1$  now, keeping all correlators normalized to unity at  $\tau = t - t_w = 0$ . Figure 2 shows results for  $\phi_{t_w}(\tau)$ , the schematic waiting-time dependent correlator calculated via Eq. (23) (replacing the general correlation functions  $C_e$  and  $C_{t_w}$  with the schematic ones,  $\phi_e$  and  $\phi_{t_w}$ , omitting the  $t_w$ -subscript only for the transient function  $\phi$ ). A glassy state was chosen,  $\varepsilon = 10^{-3}$ , so that  $\phi_e(\tau)$  attains a finite long-time limit  $f$ , and the decay of  $\phi_{t_w}(\tau)$  as  $\tau \rightarrow \infty$  is solely due to the shear flow. In this case, the last term in Eq. (23) vanishes at long times, and the time derivative of the remaining

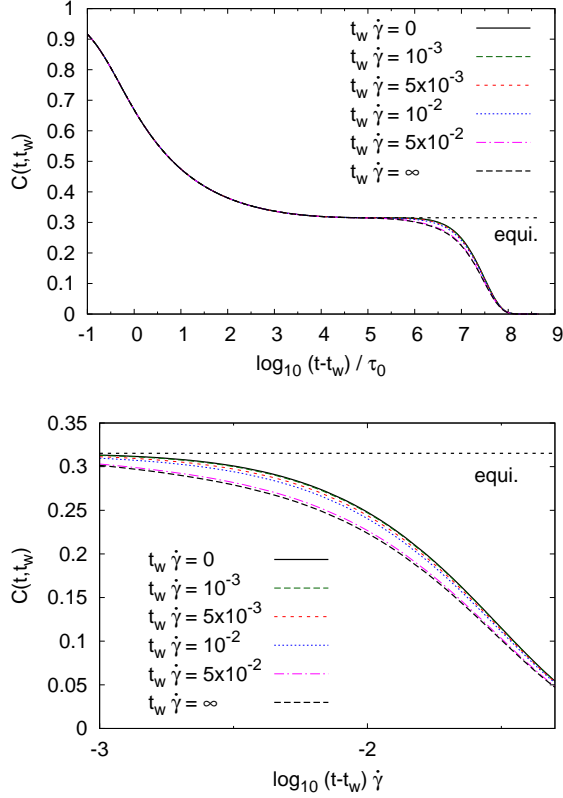


FIG. 2: Dynamical two-time correlation functions, Eq. (23), using the  $F_{12}^{(\dot{\gamma})}$  model [17] as input for the transient correlator, in the glass ( $\varepsilon = 10^{-3}$ , see text) at shear rate  $\dot{\gamma}\tau_0 = 10^{-9}$ , for various waiting times  $t_w$  as indicated (curves from top to bottom); thick lines indicate the transient ( $t_w = 0$ ) and steady-state ( $t_w = \infty$ ) correlators. The dotted line represents the equilibrium correlation function. The lower panel displays the final decay as a function of strain  $\dot{\gamma}(t - t_w)$ .

term is negative for all  $\tau$ . The decay of the transient correlator from the plateau can be well approximated by  $\phi(\tau) \approx f \exp[-(\dot{\gamma}\tau/\gamma_c)^\mu]$  with exponent  $\mu = 1.2$ , i.e. it shows “compressed exponential” behavior as a signature of the non-steady dynamics. Recall that in equilibrium colloidal suspensions,  $\mu > 1$  is excluded by the properties of the Smoluchowski operator [27, 28]. Approximating the decay for argument’s sake as a simple exponential, we immediately see that  $\phi_{t_w}(\tau) \approx \phi(\tau)(1 - \dot{\gamma}\tilde{\sigma}(t_w))$  for  $\dot{\gamma}\tau = \mathcal{O}(1)$ . Since  $\tilde{\sigma}(\infty)$  remains finite, Eq. (23) indeed describes the asymptotic approach to a steady-state correlator  $\phi_\infty(\tau)$  as  $t_w \rightarrow \infty$ . As seen in the figure, this approach occurs on a time scale  $\dot{\gamma}t_w \approx 5\%$ . The difference between steady-state and transient correlation functions becomes noticeable only once the correlation functions decay from their plateau, at  $\dot{\gamma}\tau \approx 0.001$ ; it vanishes as the functions decay to zero and is most pronounced around  $\dot{\gamma}\tau \approx 0.01$ .

In the liquid,  $\varepsilon < 0$ , similar effects as those described above are seen, but only in a regime where  $Pe = \dot{\gamma}\tau_\alpha \gg 1$ ,

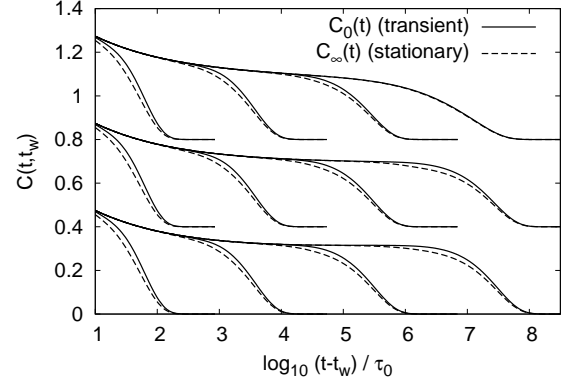


FIG. 3: Transient (solid lines) and stationary (dashed lines) correlation functions of the schematic model for three state points: top curves demonstrate  $\varepsilon = -10^{-3}$  (liquid with  $\alpha$  relaxation time  $\tau_\alpha/\tau_0 = \mathcal{O}(10^7)$ , shifted by 0.8 vertically), middle curves  $\varepsilon = 0$  (transition point, shifted by 0.4), bottom curves  $\varepsilon = 10^{-3}$  (glass). Shear rates are  $Pe_0 = \dot{\gamma}\tau_0 = 10^{-2n-1}$  with  $n = 1, \dots, 4$  (left to right).

where  $\tau_\alpha$  is a time scale characterizing the slow relaxation of the equilibrium correlator  $\phi_e(\tau)$  (the “ $\alpha$ ” time scale in glassy liquids), defining the dressed Péclet number. In this case, again, the last term in Eq. (23) can be dropped as a small correction, as  $\phi_e(\tau) \approx f$ , its plateau value, for  $\tau \approx 1/\dot{\gamma}$ . This is visualized in Fig. 3, where results for various  $\varepsilon$  and different shear rates  $\dot{\gamma}$  are shown. For  $Pe \gg 1$  (and  $Pe_0 \ll 1$ ), curves on both sides of the glass transition show qualitatively identical evolution with  $t_w$ . However, in the liquid, a linear-response regime exists for  $Pe \ll 1$ , where Eqs. (28) describe a transient correlator that is itself unaffected by shear,  $\phi(\tau) \approx \phi_e(\tau)$ . This is exemplified by the top right curve of Fig. 3, where a liquid state of the  $F_{12}$  model with small shear rate corresponding to  $Pe = \dot{\gamma}\tau_\alpha = 10^{-2}$  was chosen. Equation (23) then correctly describes the fact that all  $t_w$ -dependent correlation functions are equal. Note that this holds possibly only up to a normalization expressed by  $\alpha(t_w)$ , reflecting the fact that the static structure may be distorted by shear.

In the ideal glass, the quiescent relaxation time is infinite, and hence no linear-response regime exists. Instead, the transient correlator  $\phi(\tau)$  decays on a time scale  $\mathcal{O}(1/\dot{\gamma})$  for arbitrarily small shear rates. Hence, for large enough  $\dot{\gamma}\tau$  and  $\dot{\gamma} \rightarrow 0$ , Eq. (23) becomes invariant under the transformation  $\tau \mapsto \dot{\gamma}\tau$  and  $t_w \mapsto \dot{\gamma}t_w$  in the glass. This yields a nontrivial prediction, namely that the difference between transient and steady-state correlators in the shear-molten glass does *not* vanish as  $\dot{\gamma} \rightarrow 0$ . Rather, a scaling limit is exhibited if one considers the correlation functions on rescaled times  $\dot{\gamma}\tau$ , where both the transient and the stationary correlators attain (different) master curves. The approach to this scaling is demonstrated by Fig. 4, where the  $\varepsilon > 0$  curves of Fig. 3 are repro-



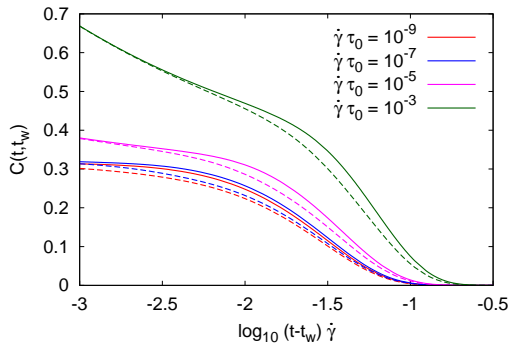


FIG. 4: Transient (solid) and stationary (dashed lines) correlators of the schematic model in the glass,  $\varepsilon = 10^{-3}$ , for shear rates  $Pe_0 = 10^{-2n-1}$ ,  $n = 1, \dots, 4$ .

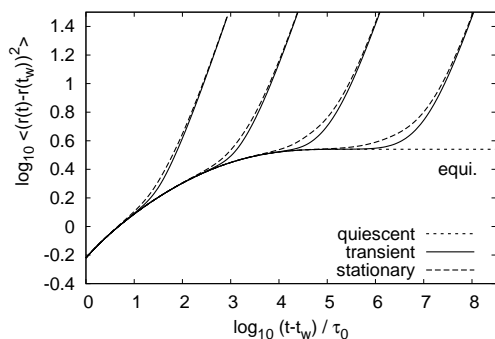


FIG. 5: Transient (solid) and stationary (dashed) mean-squared displacements in the schematic model, Eq. (30) and Eq. (25), for a glassy state,  $\varepsilon = 10^{-3}$ , with shear rates  $Pe_0 = \dot{\gamma}\tau_0 = 10^{-2n-1}$ ,  $n = 1, \dots, 4$  (from left to right). The quiescent equilibrium MSD is shown as a dotted line.

duced as functions of  $\dot{\gamma}\tau$ . One clearly identifies the approach to two master functions looking at the lowest two shear rates,  $\dot{\gamma}\tau_0 = 10^{-9}$  and  $\dot{\gamma}\tau_0 = 10^{-7}$ . One notes also that the scaling is only approached for rather small shear rates, and thus not easily verified. Although this nonanalytic limit presents an interesting test of MCT, it will in general be difficult to probe in simulation, as one would need to construct transient correlation functions in the properly ensemble-averaged glassy initial state. The physical reason behind this nonanalytic limit is the existence of a dynamical yield stress predicted by the theory, rendering the  $\dot{\gamma} \rightarrow 0$  limit under steady shear a singular one.

Figure 4 demonstrates another preasymptotic effect of the limit of vanishing shear rate: identifying the regime of accumulated strain where transient effects are largest, we found  $\dot{\gamma}\tau \approx 0.01$  from the small-shear-rate regime discussed above. However, at larger shear rates, this regime shifts to almost  $\dot{\gamma}\tau \approx 0.1$ ; these are the 10% strain corresponding to a typical localization length of hard-core particles in the glass, argued for in Ref. [1].

For the mean-squared displacements, via Eq. (25), a very similar discussion holds, as exemplified by Fig. 5. The qualitative differences between equilibrium, transient, and steady-state MSD curves is the same as for the correlators (although now, for obvious reasons, the functions increase, rather than decrease, with increasing  $t_w$  for fixed  $\tau$ ). The behavior is also in qualitative agreement with experimental and computer-simulation results of Ref. [1]. However, there, an intriguing super-diffusive regime for the transient MSD was observed which is missing in our schematic model. It can be argued that this is due to Eq. (30), where we model the memory kernel of the MSD by a strictly positive function  $\bar{m}^s(a)$ , whereas the true memory kernel leading to a superdiffusive regime should exhibit a small time window of negative values. Indeed, superdiffusive behavior was found in Ref. [1] to be connected with the stress overshoot phenomenon (not modeled in our schematic approach) that was argued to enter  $\bar{m}^s(a)$  via a generalized Stokes-Einstein approximation. Thus, the qualitative agreement of the  $t_w$ -evolution of MSD curves between our model and the simulation data highlights that the superdiffusive motion is not necessarily connected to the physics of crossing over from equilibrium to steady state after switching on shear flow.

## V. COMPARISON WITH COMPUTER SIMULATION

We now turn to a discussion of the waiting time dependence of  $C_{tw}(\tau)$  as found in computer simulation.

We first report the findings from a stochastic-dynamics computer simulation for a two-dimensional system of hard disks. To avoid crystallization, an equimolar binary mixture with diameters  $\sigma = 1$  (taken as the unit length) and  $1.4\sigma$  is chosen; this is the same system as studied earlier in steady state [29]. The number density is conveniently expressed as the packing (area) fraction of the system  $\varphi$ . Previous simulations found a glass transition at packing fractions around  $\varphi \approx 0.8$ .

The simulation is modeled after the so-called event-driven Brownian-dynamics (ED-BD) algorithm [30]; this algorithm provides an approximate solution to the stochastic differential equation underlying Eq. (4) without shear flow,

$$0 = -\zeta dx + dF^r, \quad (31)$$

where  $x$  is the configuration-space vector describing the particle positions,  $\zeta$  is a friction coefficient and  $F^r$  is a random white-noise force obeying the fluctuation-dissipation theorem,  $\langle F_i^r(t) F_j^r(t') \rangle = 2k_B T \zeta \delta(t - t') \delta_{ij}$ . Setting the amplitude of the noise correlation to unity fixes the unit of time. The interaction among the hard-sphere particles translates into boundary conditions that no two spheres overlap at any point in time. The ED-BD algorithm is, in essence, a rejection-free hybrid Monte-Carlo scheme that works by selecting a small time step  $\Delta t$ , during which a free Brownian particle undergoes

a displacement with variance  $\langle \Delta x^2 \rangle = 2D_0\Delta t$  in each Cartesian direction. Trial moves are first drawn according to the Gaussian distribution of that variance, and then corrected for unphysical overlaps. The overlap removal is performed by assigning to each originally drawn displacement  $\Delta x$  a tangent vector  $u = \Delta x/\Delta t$  and a linear curve parameter  $s \in [t, t + \Delta t]$ . Particles are then displaced along the tangent vectors by a linear mapping from  $s = t$  to  $s = t + \Delta t$ . Whenever at some  $s_c$  two particles  $i$  and  $j$  start to overlap, the corresponding trial vectors  $u_i$  and  $u_j$  are reflected along the plane perpendicular to the particles' separation vector, which ensures no-flux boundary conditions on the spheres' surfaces if  $\Delta t$  is small enough. Effectively, this translates into performing “elastic collisions” with the  $u_i$  and  $u_j$  treated as velocity vectors. The procedure is continued, taking care of all of the possibly many  $s_c$  in the same fashion until  $s = t + \Delta t$ . One is then guaranteed to have a new configuration that is overlap-free and that the phase space is sampled ergodically by diffusive motion of a free diffusion coefficient  $D_0 = \Delta t/2$ . [36].

Linear shear flow is incorporated in this algorithm following Ref. [29] by shifting the center of the distribution from which displacements are drawn by the known free-particle drift term. The translation into elastic collisions as in the flow-free case still ensures ergodicity of the algorithm and can be expected to be a reasonable approximation for small  $\dot{\gamma}\Delta t$ . Lees-Edwards boundary conditions allow to match the resulting linear velocity profile with the periodic images of the simulation box.

For the simulations presented here, we chose a time step  $\Delta t = 0.01$ , resulting in  $D_0 = 0.005$ . Initial configurations have been allowed to equilibrate during runs of up to  $D_0t/\sigma^2 = 4 \times 10^4$ , equivalent to  $2 \times 10^8$  Brownian time steps. After equilibration, shear flow was instantaneously switched on, and correlation functions have been measured for several waiting times  $t_w$  thereafter. To improve statistics, the procedure has been repeated for 300 independent runs at each density and shear rate.

Figure 6 shows the self-intermediate scattering functions for various wave vectors in the gradient direction, at packing fraction  $\phi = 0.79$ , and for a fixed shear rate  $\dot{\gamma} = 0.02D_0/\sigma^2$  ( $Pe_0 = 0.02$ ). The quiescent correlation functions are shown for comparison as dashed lines; they decay about two orders of magnitude slower than the shear-decorrelated ones, hence  $Pe \approx 10^2$ . Different waiting times are shown in dimensionless units  $\dot{\gamma}t_w$ , the scaling expected from our theoretical observations above. One recognizes from the figure the same qualitative trends as found in the Newtonian-dynamics simulation of Ref. [1] and consistent with our theory: the difference between the various waiting-time dependent correlation functions is most pronounced at intermediate times, when the functions start to decay from their respective plateaus. Following switch-on, the transient correlation function stays close to its equilibrium counterpart up to  $\dot{\gamma}\tau \approx \mathcal{O}(0.01)$ , although deviations set in earlier for higher  $q$ . This is consistent with the picture that

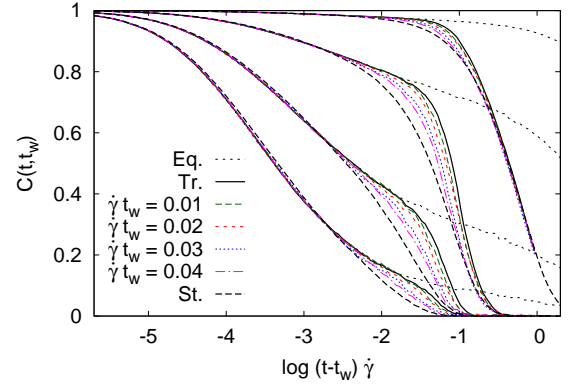


FIG. 6: Tagged-particle density correlation functions from stochastic-dynamics computer simulation of a two-dimensional hard-disk system at area fraction  $\phi = 0.79$ , just below the glass transition, and shear rate  $Pe_0 = 0.02$ . Curves from top to bottom correspond to wave numbers  $q\sigma = 1.5, 4.8, 9.7$ , and  $14.6$ , for wave vectors in the direction perpendicular to the flow direction. Thick solid and dashed lines are transient ( $t_w = 0$ ) and stationary ( $t_w \rightarrow \infty$ ) correlators, respectively. Thin lines represent different  $t_w > 0$  as indicated, the dotted curves are quiescent equilibrium correlators.

for fluctuations probing smaller length scales, smaller accumulated strains are needed to deviate from the quiescent state. Increasing  $t_w$ , the stationary correlator is approached for  $\dot{\gamma}t_w \gtrsim 0.1$ , somewhat later than in the schematic model discussed above. This results since in the simulation, also the startup stress  $\sigma(t_w)$  approaches its steady-state value later than in the schematic model (see the discussion of Fig. 8). The stationary correlation function deviates earlier from the equilibrium one than the transient one, and decays slower; generally all  $t_w$ -dependent correlation functions are found to merge again at longer times. We note in passing that the long-time decay of the transient correlation function could be fitted with a “compressed” exponential function, resulting in exponents  $\mu = 1.1, 1.8, 1.8$ , and  $1.4$  for the four different wave-vectors shown. In the corresponding MD simulation of Ref. [1], values of  $\mu$  ranging from 1.2 to 2.4 have been found, increasing with increasing wave number [31].

Figure 7 displays the mean-squared displacements obtained from the ED-BD simulation, for fixed packing fraction  $\phi = 0.79$ , but various shear rates  $\dot{\gamma}$  covering the regime  $Pe > 1$ . Again in qualitative agreement with previous Newtonian-dynamics results, and also with MSD curves obtained from confocal microscopy on colloidal suspensions [1], for fixed  $\dot{\gamma}$ , the curves for different  $t_w$  all collapse for short and for long times onto the steady-state curve, deviating at intermediate times; the transient MSD in the simulation deviates from the equilibrium curve at  $\dot{\gamma}\tau \approx 0.02$  and crosses over to the steady-state curve via a super-diffusive regime. Determining an effective exponent via the logarithmic derivative of the MSD,  $d \log \delta r^2(\tau)/d \log \tau$ , for the largest  $\dot{\gamma}$  shown in

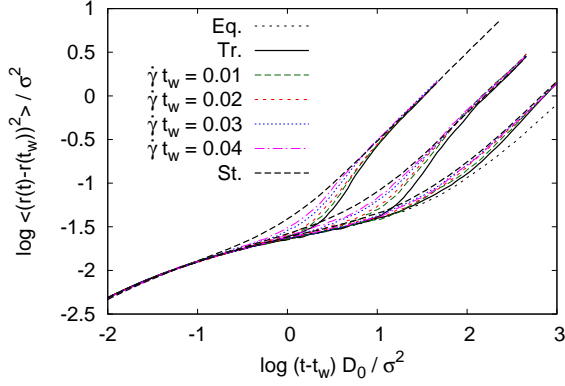


FIG. 7: Mean-squared displacements in the shear-gradient direction for the stochastic-dynamics computer simulation of a hard disk system at area fraction  $\varphi = 0.79$ , as in Fig. 6, but for different Peclet numbers,  $Pe_0 = 2 \times 10^{-2}$ ,  $2 \times 10^{-3}$  and  $2 \times 10^{-4}$  from left to right. Dotted line: quiescent equilibrium MSD.

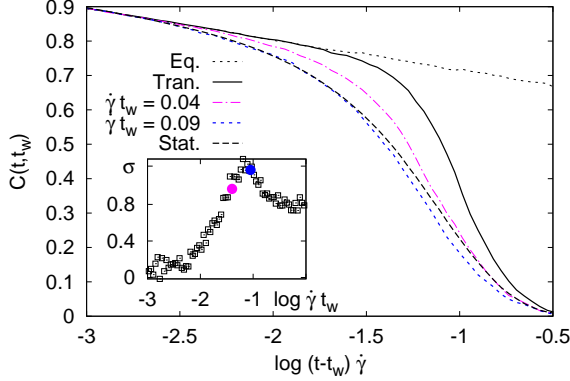


FIG. 8: Waiting-time dependent tagged-particle density correlation functions for a two-dimensional hard-disk system undergoing stochastic dynamics, as in Fig. 6 for  $q\sigma = 4.8$ , but for different waiting times corresponding to accumulated strains  $\dot{\gamma}t_w$  where a stress overshoot is seen, marked in the inset.

Fig. 7 yields  $\delta r^2(\tau) \approx \tau^{1.9}$ , comparable with the exponent found in Ref. [1] for the colloidal suspension, slightly smaller than the one extracted from the Newtonian dynamics simulation ( $\approx 2.1$ ).

The results shown in Figs. 6 and 7 are to be compared to the schematic-model results shown in Figs. 2 and 5. Regarding the cross-over from transient to stationary correlation functions, the agreement is indeed qualitative. This holds despite the fact that, as mentioned above, the schematic model we employed misses the superdiffusive regime in the MSD for technical reasons.

In the schematic model,  $\tilde{\sigma}(t_w) > 0$  is a monotonically increasing function of  $t_w$ . We hence get a sequence of

decreasing  $C_{t_w}(\tau)$  for increasing  $t_w$  shown in Fig. 2, i.e.,

$$C_{t_{w1}}(\tau) \geq C_{t_{w2}}(\tau), \quad \text{for } t_{w1} \leq t_{w2}, \quad (32)$$

or reverse for the mean-squared displacement. This ordering rule is well obeyed by the curves shown in Fig. 6, and the related ordering of the MSD is verified in Fig. 7. Note however that in simulations as well as in the microscopic MCT the startup stress exhibits an overshoot connected to a small negative dip in the transient dynamical shear modulus [1, 17], rendering  $\tilde{\sigma}(t_w)$  nonmonotonic as a function of  $t_w$ . Hence the ordering of the correlation functions given in Eq. (32) could in principle be violated for a small  $t_w$ -window, compare Eq. (23). In particular,  $C_{t_w}(\tau)$  for some fixed  $t_w = \mathcal{O}(0.1/\dot{\gamma})$  could conceivably be smaller than the steady-state correlator. In the schematic model, this effect is not contained.

However, as shown by Fig. 8, our simulation indeed indicates such a crossing of correlators as a function of  $t_w$ . Here, waiting times were chosen to sample the  $\dot{\gamma}t_w$  region around the stress overshoot. For  $t_w$  corresponding to the maximum stress,  $C_{t_w}(\tau)$  is found to fall below the stationary correlator, while this is not the case for smaller  $t_w$ . While lending credibility to our approximations, Fig. 8 also indicates that the approximation in Eq. (23) of factorizing  $\tilde{\sigma}(t_w)$  is an oversimplification. For example at  $\dot{\gamma}t_w \approx 0.04$ , the startup stress measured in the simulation reaches its steady-state value for the first time, before entering the overshoot region, and still, the corresponding correlator  $C_{t_w}(\tau)$  differs from the stationary  $C_\infty(\tau)$ .

The absence of the stress overshoot in our schematic model also implies that the stationary stress is reached earlier; waiting times of the order  $\dot{\gamma}t_w \approx 0.1$  were sufficient to enter the stationary regime in Fig. 2. In the simulation, the corresponding  $t_w$  are slightly larger, since one has to wait for the stress-overshoot region to be surpassed. The latter causes the transient correlation functions to approach the steady-state ones only for  $\dot{\gamma}t_w \approx 1$ .

Motivated by the qualitative agreement, we now turn to a more general test of Eq. (23), by checking the predicted relation among the three correlation functions (equilibrium, stationary, and finite  $t_w$ ) for the simulation data. This will be done both for the Brownian-dynamics data set just discussed, and also for the Newtonian-dynamics simulation data found in Ref. [1], in order to test the generality of our approximation regarding different forms of the short-time dynamics.

In performing the comparison to follow, we are burdened by the fact that the calculation of  $C_{t_w}(\tau)$  from  $C_0(\tau)$  and  $C_e(\tau)$  performed with experimental or simulation data is quite unstable, due to the roughening effect of the numerical derivative and a cancellation of small terms when all correlators are close to their plateau values. In the schematic model,  $C_0(\tau)$  and  $C_e(\tau)$  were available with high enough precision. We therefore have to turn toward Eq. (26) and, for the MSD, Eq. (27). Although mathematically identical, these forms give fewer numerical difficulties, as the differentiation can be replaced by

a much smoother numerical integration. Unfortunately, this makes the procedure somewhat less intuitive: given  $C_e(\tau)$  and  $C_{t_w}(\tau)$  for some  $t_w$ , we can now calculate the transient correlator  $C_0(\tau)$  but will, due to the nature of the approximations involved or due to numerical inaccuracies, get differing predictions for  $C_0(\tau)$  from different  $t_w$ . This will thus test the accuracy of our approximations for different  $t_w$ .

In addition,  $\tilde{\sigma}(t_w)$  appearing in Eqs. (26) and (27) is in general not known or easily determined. However, for small  $t_w$ , it can be replaced by its first order expansion, and we have a parameter-free prediction for  $C_0(\tau)$  out of  $C_e(\tau)$  and  $C_{t_w}(\tau)$  that we test in the next section. After that, we turn to the case  $t_w \rightarrow \infty$ , to demonstrate with  $\tilde{\sigma}(\infty)$  taken as a (wave-vector independent) fit parameter the qualitative agreement of our result with the data.

### A. Small Waiting Times

Figure 9 demonstrates the quality of our approximation, Eq. (23), for small waiting times, where  $\tilde{\sigma}(t_w) = t_w + \mathcal{O}(t_w^2)$  holds. Both Brownian dynamics and MD simulation results were used to probe the relation among the three correlator types via Eq. (26). For the ED-BD simulation, the density is given by  $\varphi = 0.79$ , and  $Pe_0 = 0.02$ , as in Fig. 6. For the MD, the temperature is given by  $T = 0.14$  (close to the glass transition on the fluid side) and  $\dot{\gamma}\sqrt{(m\sigma^2)/\epsilon} = 6 \times 10^{-4}$ , where  $\epsilon$  sets the particle interaction strength, see Ref. [1] for details. Note that in the figure, several wave vectors  $\mathbf{q}$  in the gradient direction were chosen. Recall that in Eqs. (23) and (26), the wave-vector dependence is only implicit through that of  $C_e(\tau)$  and  $C_{t_w}(\tau)$ . Since the projection onto stresses becomes exact for small waiting times, see Eq. (17), Fig. 9 shows explicitly the accuracy of our approximation for the waiting time derivative, Eq. (21). Noting that this approximation was central for the derivation of nontrivial fluctuation-dissipation-ratios in Refs. [11, 15] gives strong support for the validity of the results found there: Fig. 9 points out that this approximation captures well the observable dependence, at least for the tagged-particle correlation functions we study. Let us emphasize again, that for this comparison, no free parameter appears in the equations, as  $\alpha(t_w) = 1$  holds for tagged-particle density fluctuations, and  $\tilde{\sigma}(t_w)$  can be expanded to first order in  $t_w$ . Nevertheless, both ED-BD and MD simulation data for the transient correlation function show excellent agreement with the curve calculated via Eq. (26).

A similarly good agreement is found for the mean-squared displacements in the directions perpendicular to the shear flow, as demonstrated by Fig. 10, again for both Brownian dynamics and MD simulation. In the latter, to improve statistics, the MSD has been averaged over both the  $y$ - and  $z$ -direction. The figure in particular highlights that the failure to reproduce superdiffusive MSDs is completely within the schematic model we chose to illustrate the equations in Sec. IV. Similar to above, the

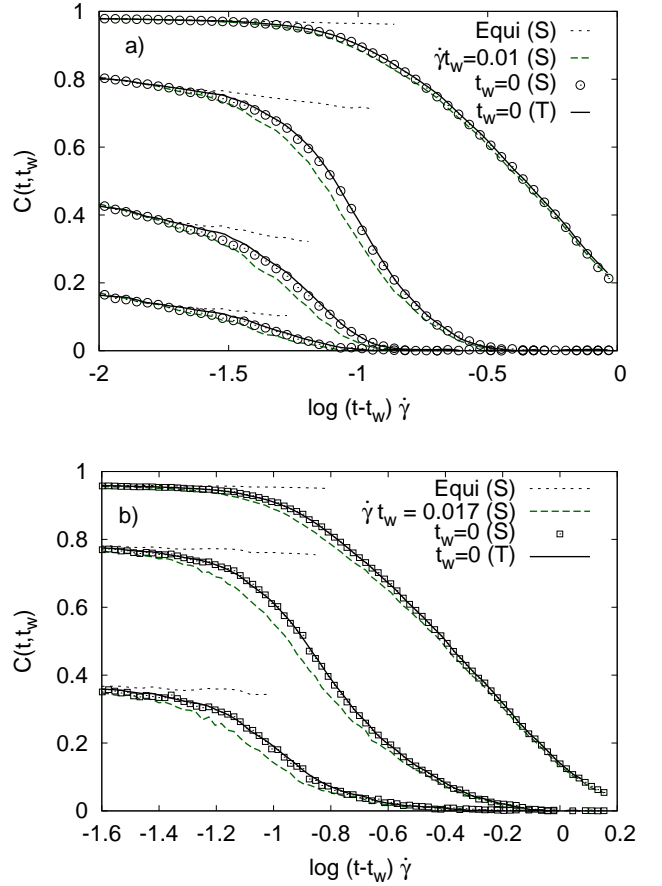


FIG. 9: (a) Parameter-free calculation of the transient correlation function from Eq. (26) from event-driven Brownian-dynamics (ED-BD) computer simulation of hard disks: dotted and dashed lines are the equilibrium and small- $t_w$  correlation functions, respectively, at  $Pe \approx 100$ ,  $Pe_0 = 0.02$  and  $\dot{\gamma}t_w = 0.010$ , with parameters as in Fig. 6. Solid lines indicate the resulting  $t_w = 0$  transient as calculated from the approximation, Eq. (26), while symbols show the corresponding curves determined from computer simulation directly. (b) Same calculation, but for molecular-dynamics (MD) simulation data of Ref. [1], for a 3D binary soft-sphere mixture at  $Pe \approx 10^3$ ,  $\dot{\gamma}t_w = 0.017$ , and wave vector magnitudes  $q\sigma = 2.3$ ,  $6.0$ , and  $12.3$  (top to bottom) in the gradient direction.

approximation for the waiting time derivative contained in Eq. (25) was central in deriving the nonequilibrium Einstein relation, Ref. [32]. The accuracy of this approximation as shown in Fig. 10 hence supports the relations found there.

### B. Large waiting times

Having verified that Eqs. (23) and (25) give a quantitatively correct account for the relation between equilibrium, waiting-time dependent, and transient correlation function for short waiting times, we now turn to



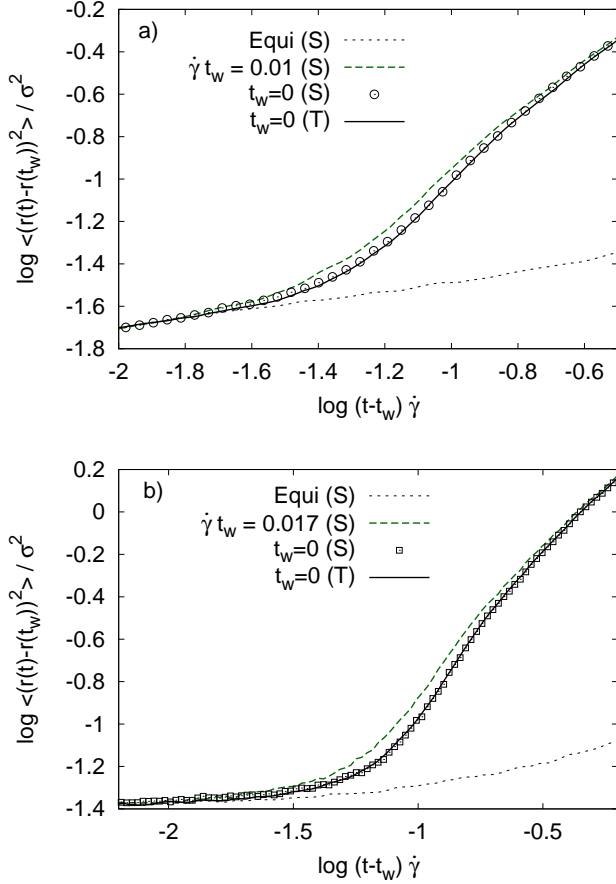


FIG. 10: Parameter-free calculation of transient mean-squared displacements from equilibrium and small- $t_w$  data via Eq. (27), parameters and symbols as in Fig. 9. (a) ED-BD computer simulation. (b) MD computer simulation.

the  $t_w \rightarrow \infty$  limit, investigating the relationship between stationary, equilibrium, and transient dynamics. We again follow the route outlined above, i.e., we determine the transient correlation functions and mean-squared displacements from the simulated equilibrium and stationary ones via Eqs. (26) and (27), and compare to the simulated transient correlation function in order to test the validity of our approach.

To continue we then need  $\tilde{\sigma}(\infty)$  entering our relation; this quantity could in principle be calculated following its definition in Eq. (14). In practice, we will use  $\tilde{\sigma}(\infty)$  as a fit parameter, noting that it should be  $q$ -independent (in general  $f$ -independent) to be meaningful.

For the Brownian dynamics data (choosing the same state point and shear rate as in the small- $t_w$  test above), we find  $\dot{\gamma}\tilde{\sigma}(\infty) = 0.04$  to give very satisfying results, shown in Fig. 11. For the molecular-dynamics simulation data,  $\dot{\gamma}\tilde{\sigma}(\infty) = 0.12$  was fitted differently, as the parameter will depend not only on the shear rate but also the details of the interaction potential. Stationary correlators have been obtained from the simulation after

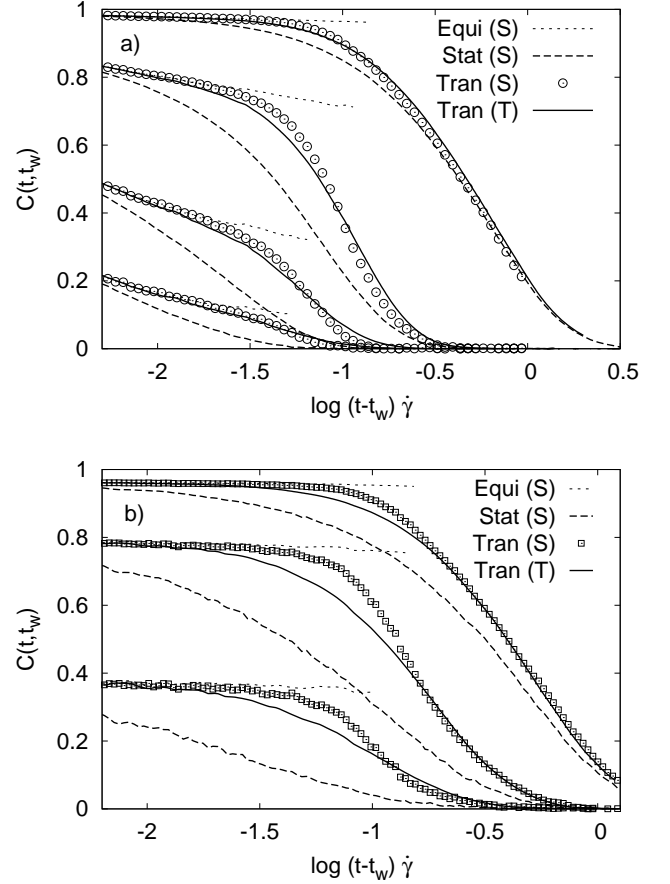


FIG. 11: Calculation of the transient correlation function from equilibrium and steady state via Eq. (26). Symbols and parameters are as in Fig. 9, but with the small- $t_w$  curve replaced by the  $t_w \rightarrow \infty$  steady-state one. The parameter  $\tilde{\sigma}(\infty)$  from Eq. (29) has been fitted. (a) Comparison with ED-BD computer simulation data with  $\dot{\gamma}\tilde{\sigma}(\infty) = 0.04$ . (b) Comparison with MD computer simulation data with  $\dot{\gamma}\tilde{\sigma}(\infty) = 0.12$ .

$\dot{\gamma}t_w = 1$ , where no significant further change with  $t_w$  was observed. As expected from the nature of our approximation, which decouples two time dependences and is hence better for small  $t_w$ , the agreement for the simulated and the calculated transient correlator is still very good, but somewhat less precise than in Fig. 9. Deviations in the comparison with Brownian dynamics simulation data are most pronounced for large  $q$ , where the predicted decay of the transient correlation function is too slow.

For the molecular-dynamics data, larger deviations occur, as exemplified in the lower panel of Fig. 11. The same qualitative trend with wave number holds as in the comparison with the ED-BD simulation, but the curve shape predicted for decay of the transient correlation function from the stationary one is markedly different from the one observed, especially in the initial decay from the plateau. Hence, while our approximation seems to hold for both ED-BD and MD equally well when applied with small enough waiting times, as in Fig. 9, it

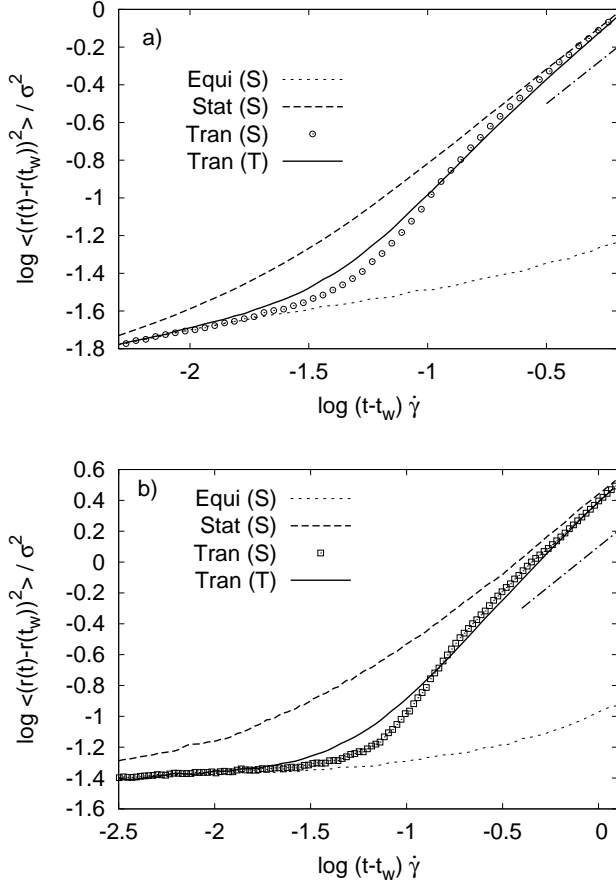


FIG. 12: Calculation of transient mean-squared displacements in the gradient direction from equilibrium and stationary curves via Eq. (27) with  $\tilde{\sigma}(\infty)$ -values as in Fig. 11. Curves correspond to the parameters as in Fig. 11. A dash-dotted line indicates a unit slope corresponding to diffusive motion. (a) ED-BD computer simulation. (b) MD computer simulation.

is more adapted to ED-BD when applied with large  $t_w$ . Let us point out that the time scale for the relaxation of the transient correlator is captured well in our approximation although it differs appreciably from the one of the stationary correlator at the larger  $q$  shown. The difference between stationary and transient correlation functions in our theory is proportional to the parameter  $\tilde{\sigma}(\infty)$ . Changing it e.g. to smaller values gives transient functions which are closer to the stationary ones in Figs. 11 (and also Fig. 12, see below).

A similar picture arises from the MSD in the gradient direction perpendicular to the shear flow, shown again for both ED-BD and MD in Fig. 12. As in Fig. 11, we have chosen  $\dot{\gamma}t_w = 1$  (ED-BD) and  $\dot{\gamma}t_w \approx 0.25$  (MD) to approximate the stationary MSD in the simulations. The transient MSDs have been calculated using Eq. (27), keeping the fit parameter  $\tilde{\sigma}(\infty)$  fixed as determined from the comparison of the correlation functions above. The agreement is then seen to be qualitative again, with some quantitative deviations mostly regarding the logarithmic

slope of the MSD at intermediate times. These deviations are larger for the MD data than for the ED-BD, and it will be interesting to explore further these differences in the waiting-time dependent evolution of sheared systems obeying different types of short-time dynamics.

It appears that, while for the transient dynamics at small  $t_w$ , possibly qualitative differences are found between MD and BD (see the discussion above in conjunction with Fig. 10), this does not seem to be the case for either the quiescent or the stationary case – the latter exemplified by the qualitative similarity of the large- $t_w$  curves in Fig. 12.

## VI. DISCUSSION

We have presented an approximate connection among the different dynamical two-point correlation functions characterizing the nonequilibrium dynamics following a sudden commencement of linear shear flow. It describes the evolution from the pre-shear equilibrium state to the stationary state attained under shear after sufficiently long waiting times.

The approximations have been derived following the integration-through transients procedure as a general tool to evaluate averages involving the unknown nonequilibrium distribution function in terms of history integrals over the known equilibrium one. ITT is exact in principle, but in evaluating the two-time three-point correlation functions, we are forced to introduce approximations. Here we have made the assumption that the dynamical variables in whose evolution we are interested in, are, in their evolution from equilibrium to steady state, dominated by an overlap with the microscopic stress tensor, or more generally the fluctuations arising from applying the nonequilibrium part of the time-evolution operator to the distribution function.

An analysis of two different sets of computer simulation data close to the glass transition for various wave numbers, shear rates, and waiting times suggests that our approximative formulas do indeed capture the essential features of the dynamical evolution from equilibrium to steady state. To test the generality of the discussed effects with respect to different short-time dynamics and dimensionality, we both analyzed previous 3D Newtonian molecular dynamics data and performed 2D event-driven Brownian dynamics (ED-BD) simulations leading to diffusive (overdamped stochastic) short-time motion.

We have made plausible the approximations by referring to a schematic model of mode-coupling theory that allows to calculate all the desired quantities numerically with high precision. The theoretical predictions are seen to broadly agree with previous results on both molecular-dynamics computer simulations and on colloidal experiments reported in Ref. [1], and also with the hard-sphere stochastic-dynamics simulations we performed. As a general trend, the transient correlation functions follow the equilibrium ones for times up to  $\dot{\gamma}\tau \approx 0.01$ ; after this

strain is reached, they deviate and decay much more rapidly in the regime of high dressed Péclet numbers we are interested in. For the tagged-particle density correlation functions, the deviation sets in earlier for larger wave number (tested in the gradient direction). For smaller  $Pe$  (or in the case of the MSD), the decisive strain is closer to  $\dot{\gamma}\tau \approx 0.1$ : as mentioned before [1], this value is suspiciously close to a typical particle localization length, supporting the picture that the steep decay of the transient correlation function marks the breaking of nearest-neighbor cages under shear. As the waiting time  $t_w$  increases, this steep decay, found to be super-exponential in our model, broadens to settle on the  $t_w \rightarrow \infty$  stationary limit for waiting times of  $\dot{\gamma}t_w \approx 1$ . For most cases, this gives rise to an ordering of  $t_w$ -dependent correlators, with the transient,  $t_w = 0$ , correlator being the largest (i.e. slowest), and the stationary,  $t_w = \infty$ , correlator being the smallest (i.e. fastest) in an intermediate window of rescaled times  $\dot{\gamma}\tau$ . However, this ordering is violated for waiting times corresponding to strains  $\dot{\gamma}t_w$  where a non-monotonic variation is observed in the shear stress after startup, the so called stress overshoot. Our approximation recovers this subtlety.

As a side note, it should be mentioned that in the case of switching on steady shear, the waiting-time dependent correlation functions are found to all decay on time scales of  $\mathcal{O}(1/\dot{\gamma})$  when leaving the linear-response regime, i.e., when  $Pe \gg 1$ . This is in notable difference to waiting-time dependences usually discussed in the aging dynamics of glasses following a sudden temperature quench or in soft-matter systems [33–35], where the final relaxation time strongly increases as a function of increasing  $t_w$ , giving rise to an ordering of correlators that is the reverse of what we discussed here.

Let us remark that our schematic-model analysis suggests to discuss the peculiarities of the transient dynamics in colloidal and non-colloidal systems in separate aspects: for both types of short-time motion “compressed exponential” relaxation is found in simulations, which in colloidal systems can be seen as the hallmark of nonequilibrium dynamics (as the equilibrium dynamics is confined to show at most exponential relaxation for any correlation function as long as only structural relaxation is involved). In fact, the nonequilibrium steady-state dynamics according to our observations is again better described by pure exponentials, so that the compressed exponentials may be the signature of nonequilibrium and non-stationary relaxation. This faster-than-exponential relaxation does, however, not directly translate into a super-diffusive (or even ballistic) regime in the mean-squared displacement, another feature observed in simulations on both types of system. As already investigated in detail in Ref. [1], this latter feature can arise independently and is directly related to the stress overshoot.

The mechanism by which the dynamics evolves from equilibrium via transient to stationary dynamics appears to have aspects that are independent on the details of the short-time motion: The points in time where de-

viations are first seen from the equilibrium correlator, and last seen with respect to the steady state, are determined by the total accumulated strain  $\dot{\gamma}\tau$ . The decisive value of  $\dot{\gamma}\tau \approx 0.1$  turns out to be suspiciously close to a typical cage size in supercooled liquids, as has been noted previously. We reiterate that this generality in the evolution from equilibrium to steady state does not mean that an equally strong statement holds as it does in equilibrium, where the long-time part of the dynamics itself is independent on the type of short-time dynamics. In fact, analyzing mean-squared displacements and tagged-particle density-correlation functions from both ED-BD and MD simulations, the MD ones appear to show a somewhat stronger transient effect than the ED-BD ones. Determining effective exponents for the MSD (from a logarithmic derivative), the MD data gives larger deviations from sub-diffusive structural relaxation. The compressed-exponential exponents obtained from the incoherent scattering function can be significantly larger than 2 in MD, but remain below 2 for the ED-BD data we analyzed. This occurs in a time window, where for the quiescent system structural relaxation prevails, and where one thus expects universal aspects of slow relaxation that are independent of the short-time dynamics. It should be noted that the simulation models are different, so that we cannot exclude the difference observed in the transients being due to details of the interparticle interactions.

Our approximation correspondingly shows largest deviations when relating equilibrium, transient, and stationary correlation functions at large  $q$  for the molecular-dynamics simulation, even though it performs surprisingly well for the same MD data when restricting it to smaller waiting times. This may indicate that the peculiar form of the  $t_w = 0$  transient in molecular dynamics is not fully captured by considering all dynamical relaxations to be governed by the dynamics of the potential part of the local stress tensor (as we did to arrive at our approximation), but that non-potential parts of the dynamics may play a role in this regime, too.

Nevertheless, the overall quality of the waiting-time-derivative approximation (Eq. (21)) is found to be remarkably accurate. This lends further support to the earlier discussion of nonequilibrium fluctuation-dissipation ratios and Einstein relations within MCT and its schematic models, as the equivalent approximations have been used there [11, 15, 32].

## Acknowledgments

We wish to acknowledge fruitful and stimulating discussions with Matthias Fuchs, Jürgen Horbach, Joseph M. Brader and Jochen Zausch. We thank Jochen Zausch for providing us with his molecular-dynamics simulation data. This work was partially supported by the Helmholtz-Gemeinschaft (HGF) through its Impuls- und Vernetzungsfonds. Th. V. acknowledges funding through

a Helmholtz-University Young Investigator Group, and through a fellowship of the Zukunftskolleg of the Universität Konstanz. M. K. acknowledges funding through the International Research Training Group “Soft Condensed Matter”, IRTG 667, as well as the Sonderforschungsbereich Transregio 6 “Physics of Colloidal Dispersions in External Fields”.

## Appendix A: Hard Spheres

For the hard sphere system, the instantaneous shear modulus diverges, rendering the projector  $\mathcal{P}_\sigma$  leading to Eqs. (13) and (14) ill-defined. For a proper treatment of this singular limit, one can use instead

$$\mathcal{P}_\sigma(s_0) = e^{\Omega^\dagger s_0} \langle \sigma_{xy} \rangle \langle \sigma_{xy} e^{2\Omega^\dagger s_0} \sigma_{xy} \rangle^{-1} \langle \sigma_{xy} e^{\Omega^\dagger s_0} \quad (\text{A1})$$

for some fixed small  $s_0$ . With this choice, Eq. (13) remains unmodified, but the insertion of  $\exp[\Omega^\dagger s_0] \mathcal{P}_\sigma(s_0) \exp[-\Omega^\dagger s_0]$  changes Eq. (14) to

$$\tilde{\sigma}(t_w, s_0) = \int_{2s_0}^{t_w} \frac{\langle \sigma_{xy} e^{\Omega^\dagger s} \sigma_{xy} \rangle}{\langle \sigma_{xy} e^{2\Omega^\dagger s_0} \sigma_{xy} \rangle} ds, \quad (\text{A2})$$

where the integrand remains finite for all  $t_w \geq 2s_0$ . The approximation thus, in the case of hard spheres, consists of coupling the variable  $f$  to the shear stress at some small cutoff time  $s_0$ .

- 
- [1] J. Zausch, J. Horbach, M. Laurati, S. Egelhaaf, J. M. Brader, Th. Voigtmann, and M. Fuchs, *J. Phys.: Condens. Matter* **20**, 404210 (2008).
  - [2] F. Varnik, L. Bocquet, and J.-L. Barrat, *J. Chem. Phys.* **120**, 2788 (2004).
  - [3] J. Rottler and M. O. Robbins, *Phys. Rev. E* **68**, 011507 (2003).
  - [4] A. Tanguy, F. Leonforte, and J.-L. Barrat, *Eur. Phys. J. E* **20**, 355 (2006).
  - [5] H. Risken, *The Fokker-Planck Equation* (Springer, Berlin, 1984).
  - [6] N. G. van Kampen, *Stochastic Processes in Physics and Chemistry* (North-Holland, Amsterdam, 1992).
  - [7] W. Götze, *Liquids, freezing and glass transition* ed J.-P. Hansen, D. Levesque and J. Zinn-Justin (Amsterdam, 1991) p 287.
  - [8] M. Fuchs and M. E. Cates, *J. Rheol.* **53**, 957 (2009).
  - [9] J. K. G. Dhont, *An Introduction to Dynamics of Colloids* (Elsevier, Amsterdam, 1996).
  - [10] M. Fuchs and M. E. Cates, *J. Phys.: Cond. Mat.* **17**, 1681 (2005).
  - [11] M. Krüger and M. Fuchs, *Phys. Rev. Lett.* **102**, 135701 (2009).
  - [12] M. Fuchs and K. Kroy, *J. Phys.: Condens. Matter* **14**, 9223 (2002).
  - [13] W. Götze and A. Latz, *J. Phys.: Condens. Matter* **1**, 4169 (1989).
  - [14] O. Henrich, O. Pfeifroth, and M. Fuchs, *J. Phys: Condens. Matter* **19**, 205132 (2007).
  - [15] M. Krüger and M. Fuchs, *Phys. Rev. E* **81**, 011408 (2010).
  - [16] R. A. Lionberger and W. B. Russel, *J. Rheol.* **38**, 1885 (1994).
  - [17] M. Fuchs and M. E. Cates, *Faraday Discuss.* **123**, 267 (2003).
  - [18] M. Fuchs and M. Ballauff, *J. Chem. Phys.* **122**, 094707 (2005).
  - [19] M. Fuchs and M. Ballauff, *J. Chem. Phys.* **125**, 204906 (2006).
  - [20] J. J. Crassous, M. Siebenbürger, M. Ballauff, M. Drechsler, D. Hajnal, O. Henrich, and M. Fuchs, *J. Chem. Phys.* **128**, 204902 (2008).
  - [21] D. Hajnal, O. Henrich, J. J. Crassous, M. Siebenbürger, M. Drechsler, M. Ballauff and M. Fuchs, *AIP Conference Proceedings* **1027**, 674 (2008).
  - [22] J. M. Brader, Th. Voigtmann, M. Fuchs, R. G. Larson, and M. E. Cates, *Proc. Natl. Acad. Sci. USA* **106**, 15186 (2009).
  - [23] W. Götze, *Z. Phys. B* **56**, 139 (1984).
  - [24] F. Varnik and O. Henrich, *Phys. Rev. B* **73**, 174209 (2006).
  - [25] M. Krüger, *Properties of Non-Equilibrium States: Dense Colloidal Suspensions under Steady Shearing* (PhD Thesis, Universität Konstanz, 2009), URL <http://nbn-resolving.de/urn:nbn:de:bsz:352-opus-80732>.
  - [26] M. Fuchs, W. Götze, and M. R. Mayr, *Phys. Rev. E* **58**, 3384 (1998).
  - [27] G. Nägele, *Phys. Rep.* **272**, 215 (1996).
  - [28] T. Franosch and Th. Voigtmann, *J. Stat. Phys.* **109**, 237 (2002).
  - [29] O. Henrich, F. Weysser, M. E. Cates, and M. Fuchs, *Phil. Trans. R. Soc. A* **367**, 5033 (2009).
  - [30] A. Scala, Th. Voigtmann, and C. De Michele, *J. Chem. Phys.* **126**, 134109 (2007).
  - [31] J. Zausch, *Dynamics, Rheology and Critical Properties of Colloidal Fluid Mixtures: Molecular Dynamics Studies in Equilibrium and Under Shear* (PhD Thesis, Universität Mainz, 2008).
  - [32] M. Krüger and M. Fuchs, *Prog. Theor. Phys. Suppl.* (accepted).
  - [33] M. E. Cates and M. R. Evans, eds., *Soft and Fragile Matter*, vol. 53 of *Scottish Universities Summer School in Physics* (IOP Press, Bristol, UK, 2000).
  - [34] L. Cipelletti and L. Ramos, *Curr. Opin. Colloid Interf. Sci.* **7**, 228 (2002).
  - [35] J.-L. Barrat, *J. Phys.: Condens. Matter* **15**, S1 (2003).
  - [36] The algorithm has originally been described as assigning pseudo-velocities to the particles and then performing Newtonian-flight sub-simulations in every time step of length  $\Delta t$ .